JOURNAL OF PHYSICAL ORGANIC CHEMISTRY, VOL. 10, 484–498 (1997)

# PHOTOINDUCED INTRAMOLECULAR ELECTRON TRANSFER IN DICHROMOPHORE-APPENDED $\alpha$-HELICAL PEPTIDES: SPECTROSCOPIC PROPERTIES AND PREFERRED CONFORMATIONS

ANDREAS KNORR, ELENA GALOPPINI AND MARYE ANNE FOX*

*Department of Chemistry and Biochemistry, University of Texas at Austin, Austin, Texas 78712, USA*

**The $\alpha$-helical structure of donor–acceptor-substituted peptides 1 and 2 was established by circular dichroism and NMR spectroscopy. The photoproduction of a spatially separated radical ion pair was detected by transient absorption spectroscopy. The expected influence of the electric field along the helical pitch direction was established by monitoring $S_1$ lifetimes. The complex kinetics of the observed decays indicate that even these rigid peptides exist in a distribution of conformations. This assertion is further supported by single-photon counting measurements, NMR spectroscopy (COSY, NOESY and variable-temperature $^1$H NMR) and extended MMS2 force-field model calculations. An estimate for the rotational thresholds of the appended chromophores was obtained, and the character of the electronic interaction between the appended chromophores was examined by semiempirical single-point calculations. Such calculations show the possible importance of through-bond interactions between the chromophores. The backbone conformational regularities of 1 and 2 are sufficient to establish the previously reported influence of a electrostatic field on photoinduced electron transfer rates, but side-chain conformational mobility of 1 and 2 imposes an inherent limitation on experimental observations. © 1997 John Wiley & Sons, Ltd.**

*J. Phys. Org. Chem.* **10**, 484–498 (1997) No. of Figures: 12 No. of Tables: 7 No. of References: 21

*Keywords:* photoinduced intramolecular electron transfer; dichromophore-appended $\alpha$-helical peptides; preferred conformations

*Received 28 May 1996; revised ?? September 1996; accepted 27 September 1996*

## INTRODUCTION

In previous work we studied the rates of photoinduced electron transfer between a *p-N,N*-dimethylanilino (Dma) and a 1-pyrenyl (Pyr) group attached to a $\alpha$-helical peptide comprised of alternating L-alaline and $\alpha$-methylalanine amino acid residues.[1] The $\alpha$-helical peptides **1** and **2** served as the models to study the effect of the electric field generated by the helix dipole on the rate of photoinduced electron transfer between the two appended groups.

In helical peptides, the dipoles of the amino acid residues, estimated to be *ca* 3·5 D each, are aligned and generate a net macromolecular dipole which can be approximated by a partial positive charge at the amino end and a partial negative charge at the carboxyl end of the peptide. This large electrostatic field, estimated from vacuum electrostatics to be $10^9$ V/m$^{-1}$ in an $\alpha$-helix, influences numerous aspects of protein function and structure and may also have a role in the primary charge separation in photosynthesis. (For a review of $\alpha$-helix dipole on protein structure and function, see Ref. 2). It has been postulated that in the bacterial photosynthetic reaction center the antiparallel orientation of the charge-separated pair (with respect to the electric field generated by the helical sections of protein) may increase the rate of electron transfer.[2a,3,4] The energy of a charge-separated pair in an electric field is affected by this orientation (Figure 1).[4d] The driving force of the reaction, and therefore the rate of photoinduced electron transfer, will increase or decrease depending on the magnitude of the field-induced dipole.

In peptides **1** and **2**, which differ only by the sequence of attachment of the chromophores with respect to the helix ends, photoinduced electron transfer generates a charge-separated radical ion pair oriented antiparallel or parallel, respectively, to the helix dipole moment (Figure 2). Peptides **1** and **2** are useful models to study this phenomenon as it is not simple to orient experimentally the dipole moment of an arbitrary peptide specifically with or against an external field.

* Correspondence to: M. A. Fox.

*Contract grant sponsor:* US Department of Energy, Office of Basic Energy Science.

 CCC 0894–3230/97/070484–15 $17.50

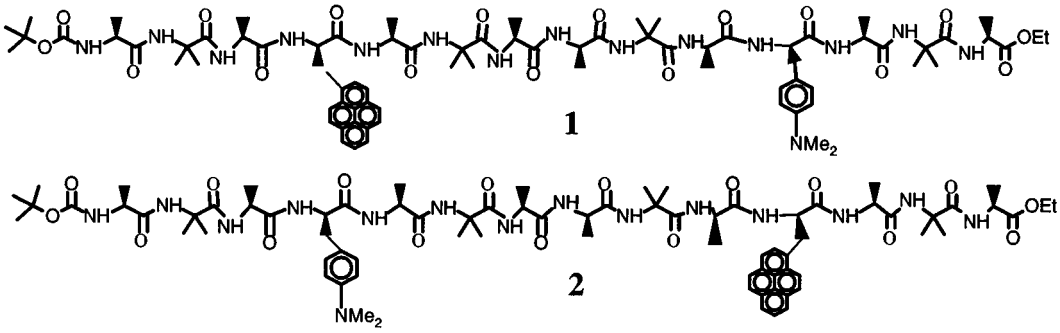


## RESULTS AND DISCUSSION

### Transient absorption spectra

In order to establish that a charge-separated ion pair is indeed formed, we studied the transient absorption spectra of **1** and **2**. The absorption maxima to be expected in this experiment are those typical of a pyrene radical anion–dimethylaniline radical cation pair in which pyrene, the excited molecule, acts as the electron acceptor and dimethylaniline, the quencher, acts as the donor. This spectrum typically exhibits maxima at 492 nm (pyrene radical anion, $Py^{-}$), 450 nm (dimethylaniline radical cation, $Dma^{+\cdot}$) and 412 nm (pyrene triplet absorption, $^{3}Py^{\star}$). In a control experiment, we obtained the transient absorption spectrum of pyrene–dimethylaniline (intermolecular electron transfer quelching) in the same solvent and experimental conditions used to obtain the spectra shown in Figure 4. Transient absorption spectra obtained for the intermolecular electron transfer quenching in pyrene–dimethylaniline in $CH_3CN$ (Ref. 5). The last absorption is produced at least in part by radical ion recombination, as is supported by the observation of its characteristic lifetime and by a correlation of the appearance of the 412 nm triplet absorption with decay of the two radical-ion transients).[5a]

The transient absorption spectra of **1** and **2** in $CH_3CN$ (Figure 3) were obtained by laser flash photolysis ($\lambda_{exc}$ = 355 nm, pulse width = 12 ns, laser power 100% = 8·7 mJ). The solutions were carefully degassed by six freeze–pump–thaw cycles, since bubbling with argon for 20 min before and during the experiment still left sufficient residual oxygen to lead exclusively to pyrene triplet formation. Data were collected every 10 nm in the wavelength range 370–550 nm in the 200 μsec time-scale. Each point is an average of four laser pulses.

In both spectra (Figure 3), two major absoprtions are present at about 420 and 500 nm. These correspond roughly to the expected absorptions shifted slightly red by the more polar environment of the peptide backbone. The absorption at 500 nm is due primarily to the pyrene radical anion, which has fully decayed 130 μs after the laser pulse. In the spectrum of **2**, the intensity of the $Py^{-}$ absorption is relatively smaller than that in **1**. (The stronger absorption assigned to $Py^{-}$ was observed after 0·5 μs. The resolution of the laser used in this experiment was insufficient to observe the same spectral appearance in the nanosecond time regime. A smaller intensity absorption for $Py^{-}$ was detected in the spectrum of **2**, where slower electron transfer was observed. This has been explained as a consequence of the decreased stability of the radical ion pair caused by

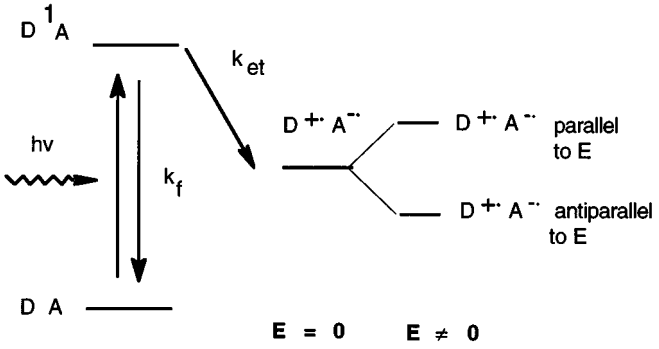


Figure 1. Energy dependence of the orientation of a charge-separated ion pair in an electric field. D = electron donor; A = electron acceptor

 

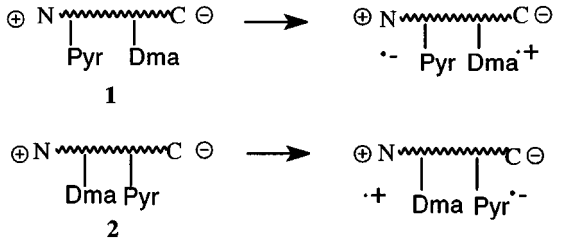


Figure 2. Formation of the charge-separated ion pair either anti-parallel (in **1**) or parallel (in **2**) to the helix electric field

unfavorable electrostatic repulsion.) In neither spectrum does the 412 nm absorption increase as the $Py^-$ signal decays. We therefore conclude that this absorption derives primarily from $^3Py^\star$ produced by intersystem crossing from the excited singlet, rather than by radical ion recombination.

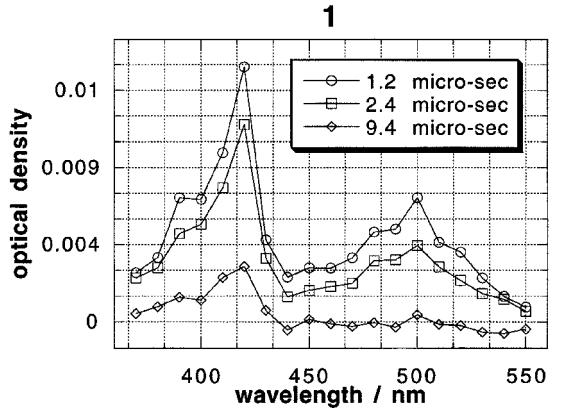


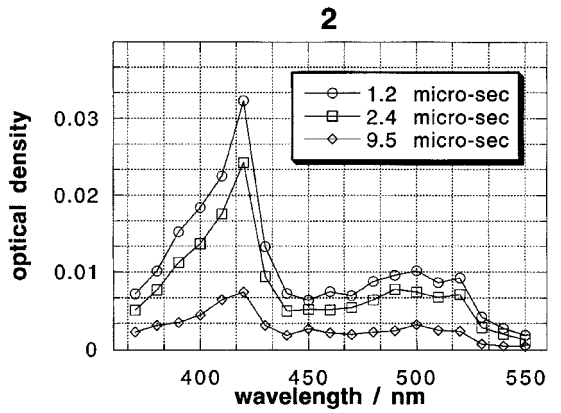


Figure 3. Absorption spectra of **1** and **2** observed (a) 11, (b) 23 and (c) 94 μs after the laser pulse. $\lambda_{exc}$ = 355 nm. Measured as $1\times10^{-4}$ M degassed solutions in acetonitrile

This implies the existence of at least some conformation(s) in which the formation of a charge-separated ion pair by intramolecular electron transfer is substantially slower than intersystem crossing.

Because both $Py^-$ and $^3Py^\star$ are present, the spectra of **1** and **2** are complicated combinations of overlapping absorptions. The weak absorption of $Dma^+$ at 450 nm is obscured by the larger absorptions of the pyrene radical anion and triplet. A kinetic analysis of the decay of the transient absorptions of **1** at 420 nm and at 500 nm (Figure 4) shows that both signals include contributions from at least two components. The same spectral complexity is also observed in the transient absorption spectrum of **2**.

In the transient absorption spectra of both **1** and **2**, the 420 nm absorption could be fit by competing second- and first-order decays, the second-order component of which had a lifetime of about 35 μs. When the excitation pulse intensity was decreased to 66%, 51% and 30% of the laser power, $\tau_{1/2}$ increased by a proportional amount, within the

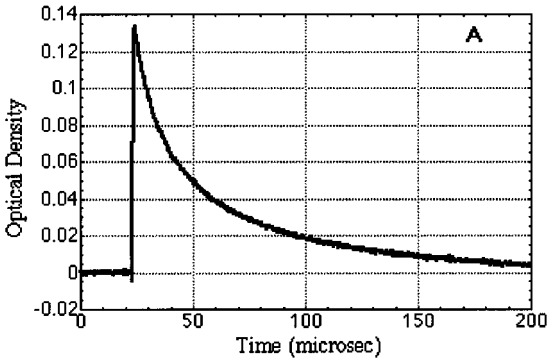


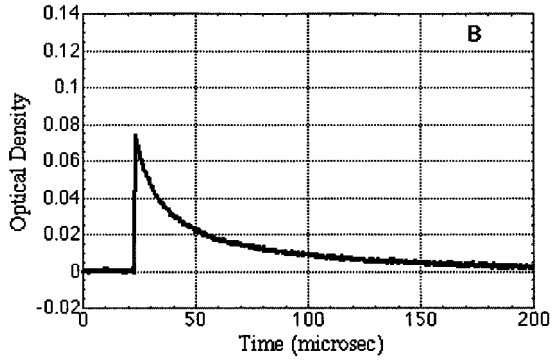


Figure 4. Decay of the transient absorption signals produced by flash excitation of **1** as a $1\times10^{-4}$ M degassed solution in acetonitrile at: (A) 420 and (B) 500 nm. Each point is an average of data collection from 10 laser pulses, collected every 10 nm. Excitation 80 mJ at 355 nm.

limit of experimental error (about 25%), as is expected for a second-order process. The lifetime of the first-order component, assigned to $^3Py^\star$, was about 200 μs (certainly there is a large error in this value because the lifetime of $^3Py^\star$ in many non-aromatic solvents has been reported as 11 ms)[6] and was unchanged as the excitation intensity was decreased (to 66%, 51% and 30% of the laser power). This observation is as expected for a first-order process. The decay of the pyrene radical anion absorption at 500 nm in the spectra of **1** and **2** could not be unambiguously fit to either competing second- and first-order decays or two first-order decays, implying an even more complex overlay of different absorptions at 500 nm. Even in the face of such complexity, the transient absorption spectra in Figure 4 provide direct evidence of the formation of a long-lived (about 100 μs) charge-separated ion pair in both **1** and **2**.

**Time-resolved fluorescence**

Previously, we have shown by a study of the time-resolved fluorescence of peptides **1** and **2** that the rates of electron transfer in **1** are 5–27 times faster than in **2**, the difference being larger in solvents of smaller dielectric constant.[1] This result is in agreement with the postulated effect of the helix dipole. However, the consistent observation of biexponential decay is a strong indication of multiple side-chain conformations of the oligopeptides in the ground state (for studies of electron transfer in peptides, see Ref. 7). In relatively short (<50 residues) oligopeptides, the backbone and/or the chromophores linked to the backbone through the methylenic units may experience some conformational mobility.[7,a,b,e] For this reason, we could not exclude the possiblity, in our original study, that the observed rate

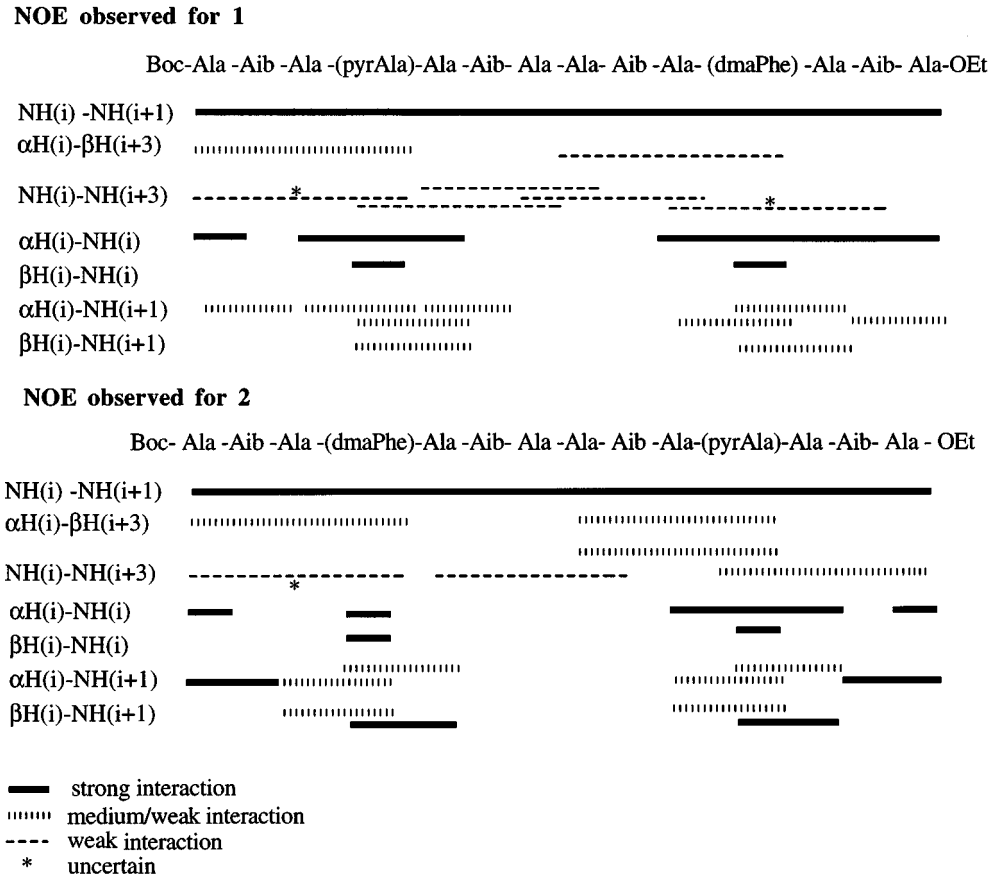


Figure 5. NOE interactions determined by COSY and NOESY correlation NMR spectroscopy of oligopeptides **1** and **2**

 

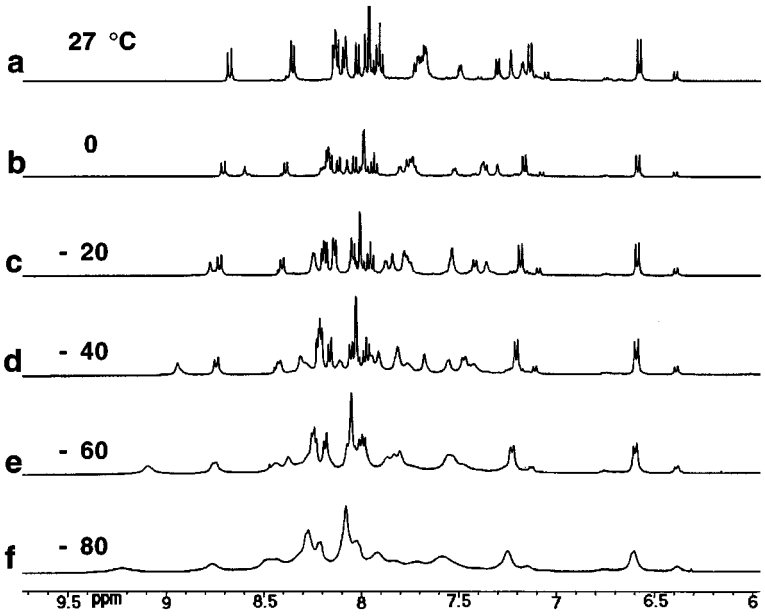


Figure 6. $^1$H NMR spectrum (6·0–9·7 ppm region) of **2** in THF from (a) 27 to (e) −80°C.

**3**

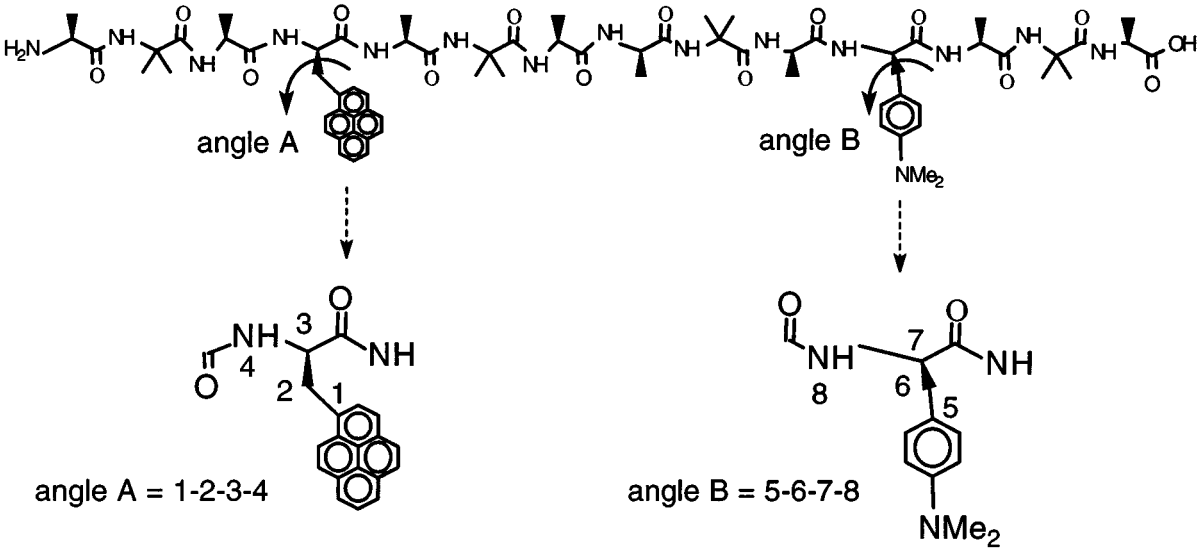


 

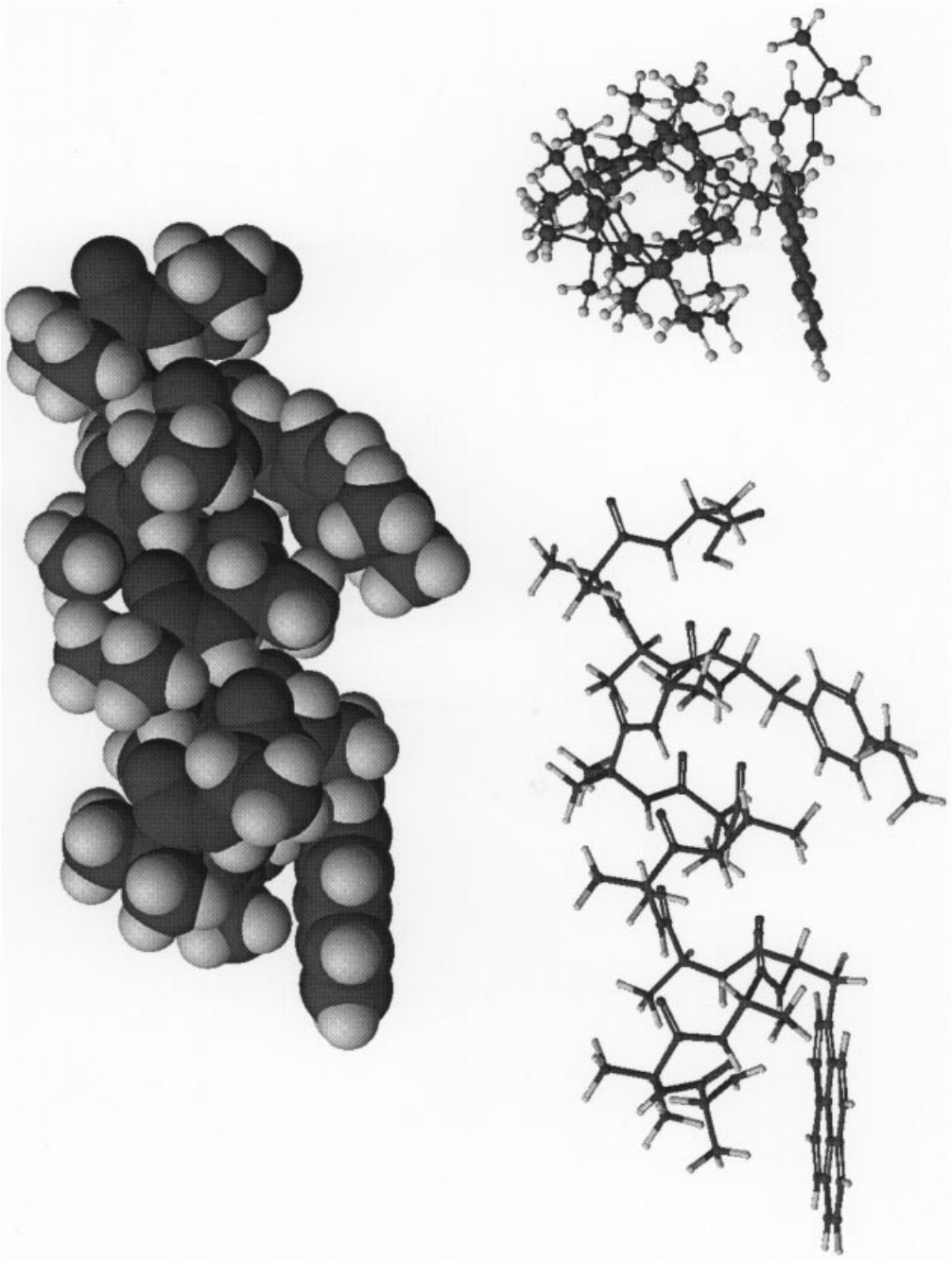

Figure 7. Force-field calculated energy minima for conformer **3a**.

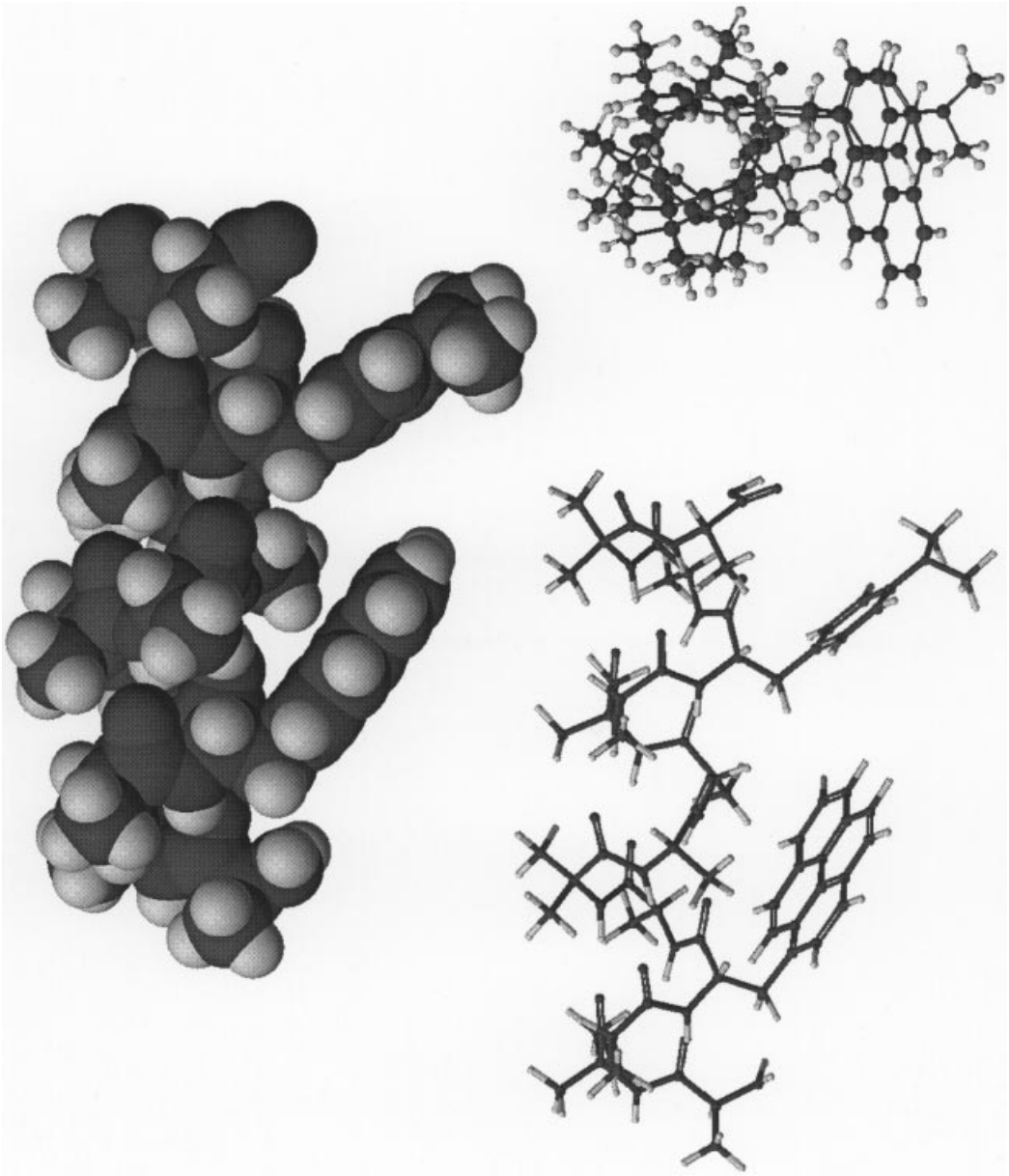

Figure 8. Force-field calculated energy minima for conformer **3b**

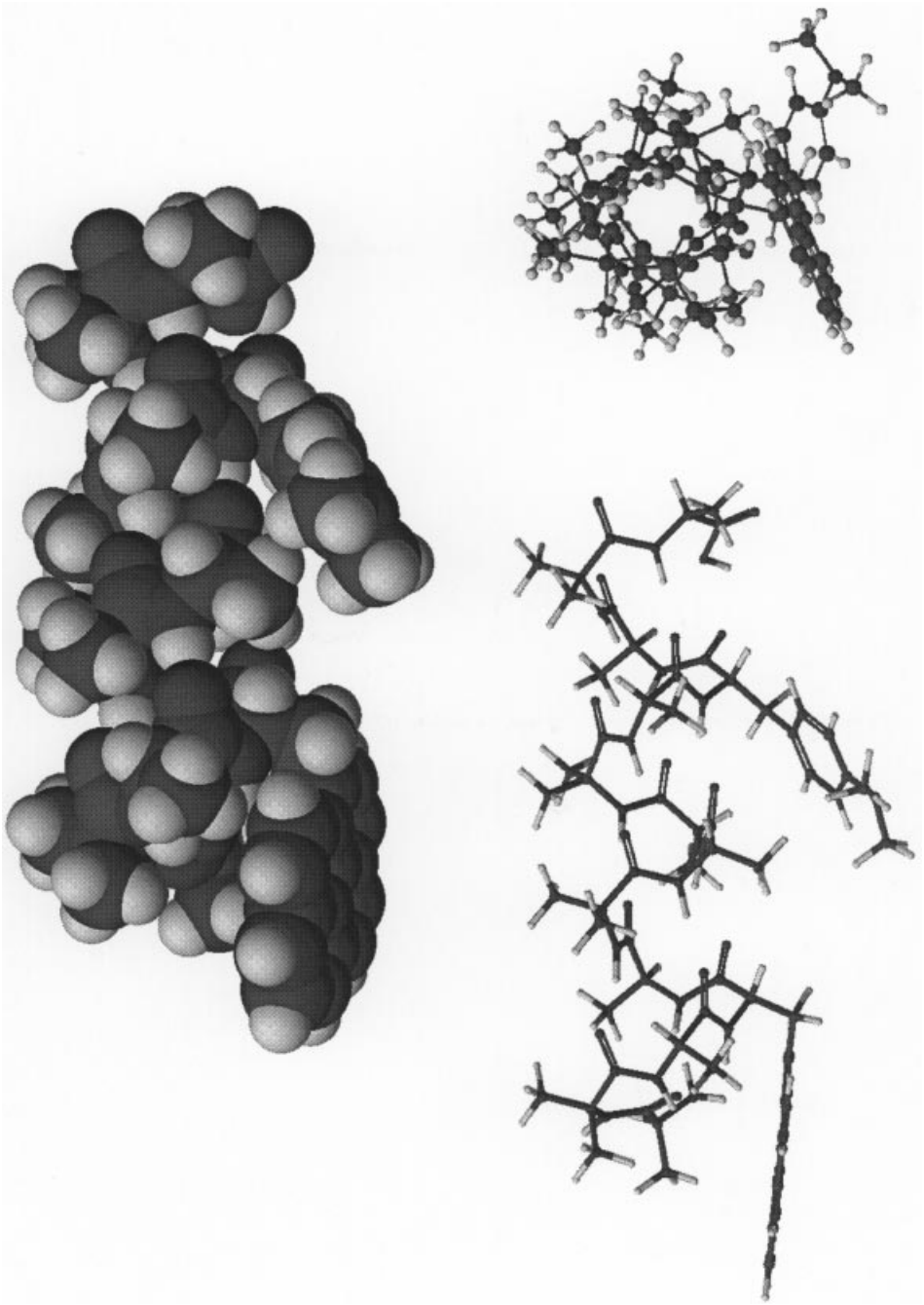

Figure 9. Force-field calculated energy minima for conformer **3c**

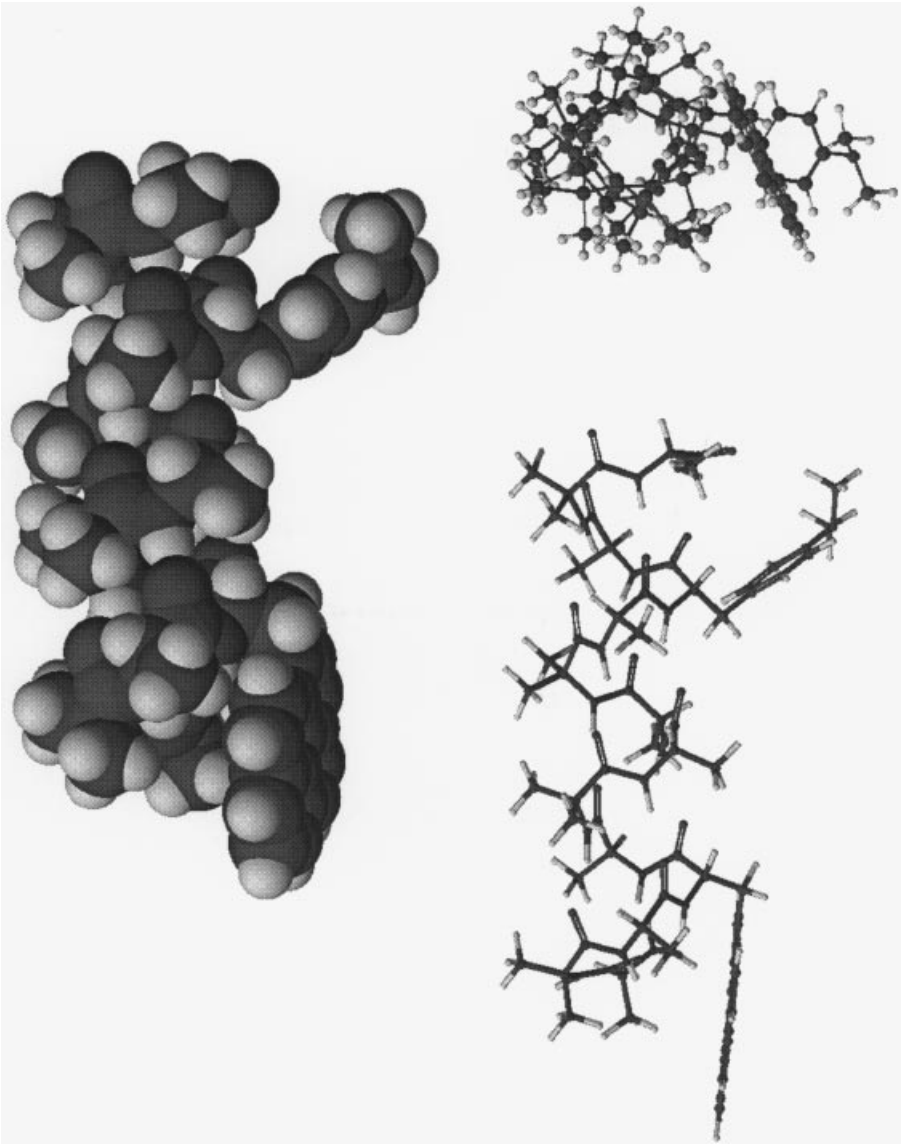

Figure 10. Force-field calculated energy minima for conformer **3d**

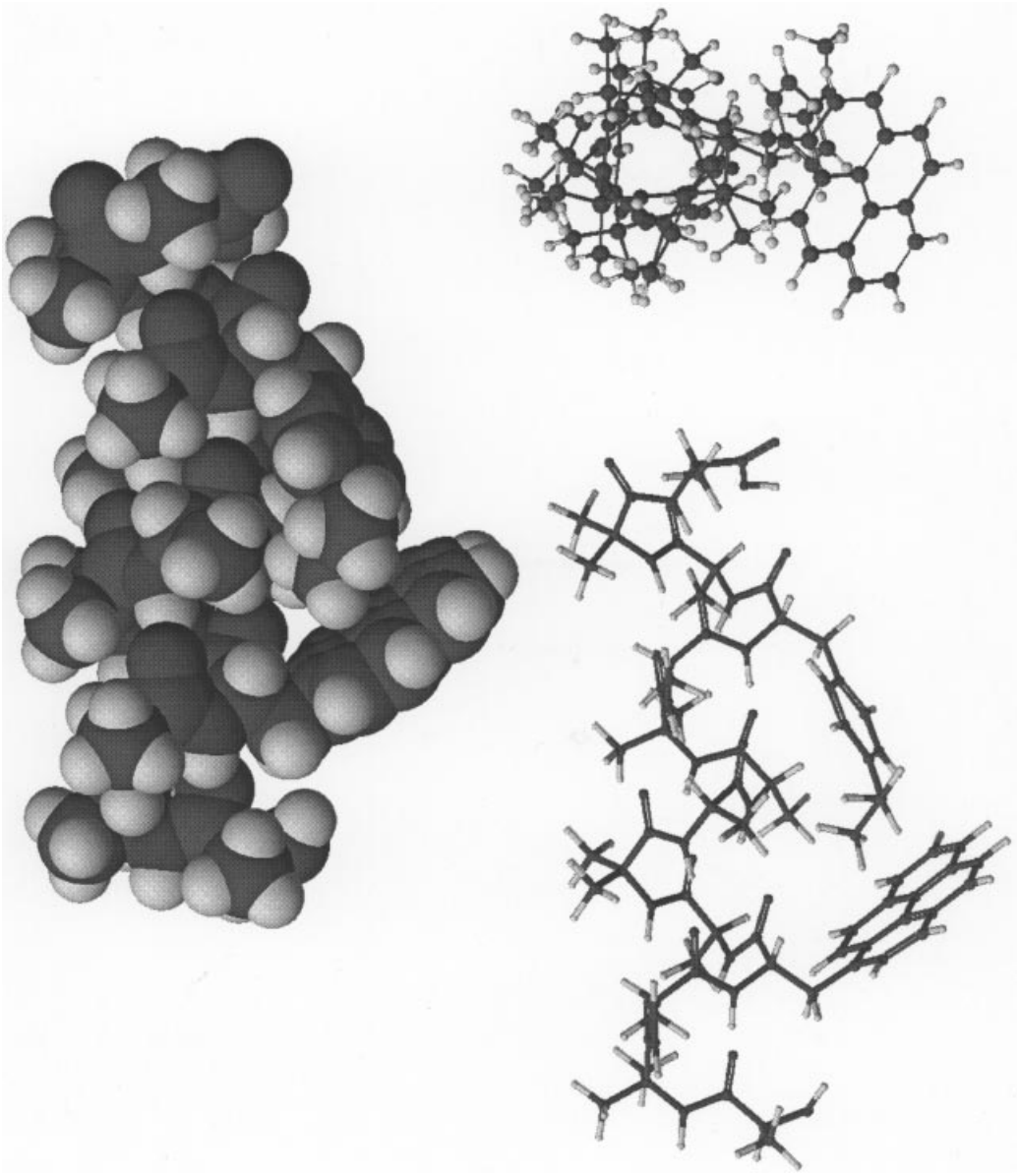

Figure 11. Force-field calculated energy minima for conformer **3e**

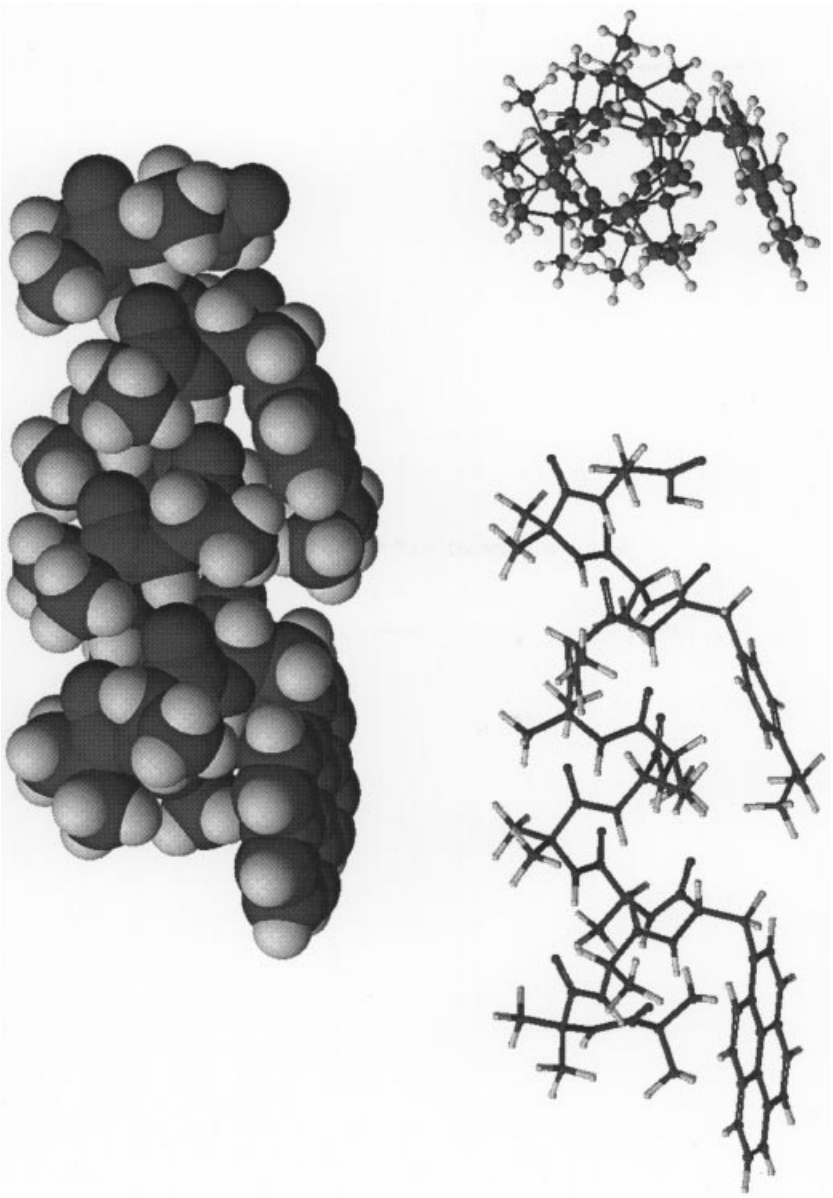

Figure 12. Force-field calculated energy minima for conformer **3f**

Table 1. Calculated heats of formation and barriers of rotation (MM2 force field)

| | | Angle B (donor) | | Angle A (acceptor) | |
|---|---|---|---|---|---|
| Conformer | Heat of formation (kcal/mol$^{-}$) | Rotation in positive direction[b] (kcal/mol$^{-1}$) | Rotation in negative direction[b] (kcal/mol$^{-1}$) | Rotation in positive direction[b] (kcal/mol$^{-1}$) | Rotation in negative direction[b] (kcal/mol$^{-1}$) |
| **3a** | −54·16 | 17·38 | 7·46 | 13·55 | 6·69 |
| **3b** | −46·33 | 2·95 | 3·36 | 5·93 | 6·94 |
| **3c** | −53·37 | 13·58 | 8·34 | 13·52 | 5·12 |
| **3d** | −49·93 | 2·93 | 6·76 | 14·00 | 5·06 |
| **3e** | −51·71 | 10·71 | 12·26 | 8·20 | 11·10 |
| **3f** | −52·47 | 11·73 | 8·38 | 8·59 | 7·61 |

[a] 1 kcal = 4·184 kJ.
[b] Δ heat of formation (rotational barrier) = heat of formation (estimated transition state) − heat of formation (ground-state conformer).

differences might be a consequence of ground-state conformational differences instead of differences caused by the macromolecular dipole.[1] In order to understand better the conformational flexibility of the chromophores, a more rigorous conformational analysis of **1** and **2** has been conducted in which circular dichroism (CD) spectra and 2D $^{1}$H NMR data are used, together with force-field and semiempirical calculations, to establish both side-chain conformations and helical structure.

## CD and NMR spectra

As the object of our study was to investigate the effect of the helix dipole on intramolecular electron coupling, it was necessary to establish whether **1** and **2** do indeed exist as α-helices. Oligopeptides composed only of alanine (Ala) are usually α-helical,[9] but dichromophore-labelled $Ala_n$ peptides with $n<4$ are insoluble in organic solvents.[9] Oligopeptides composed only of α-methylalanine (Aib) are more soluble and usually form $3_{10}$ helices, but the peptide coupling between two α-disubstituted peptides is typically a

Table 2. Calculated dipole moments (in debye) for **3a**–**f**

| Conformer | AM1 | PM3 | MNDO | MINDO-3 |
|---|---|---|---|---|
| **3a** | 45·25 | 46·34 | 42·99 | 48·05 |
| **3b** | 45·10 | 46·38 | 42·29 | 48·30 |
| **3c** | 43·92 | 45·18 | 41·69 | 47·00 |
| **3d** | 42·29 | 43·80 | 40·16 | 45·98 |
| **3e** | 44·56 | 45·71 | 41·68 | 47·58 |
| **3f** | 42·83 | 44·00 | 40·80 | 45·96 |

Table 3. Relative heats of formation (kcal/mol$^{-1}$) of **3b–f** (with respect to **3a**)

| Conformer | MM2 | AM1 | PM3 | MNDO | MINDO-3 |
|---|---|---|---|---|---|
| **3a** | 0 | 0 | 0 | 0 | 0 |
| **3b** | 7·83 | −5·43 | −2·70 | −26·43 | −24·12 |
| **3c** | 0·82 | −1·77 | 0·16 | −0·04 | 0·16 |
| **3d** | 4·23 | 0·88 | −0·03 | −8·15 | 7·19 |
| **3e** | 2·45 | −4·29 | −4·50 | −11·83 | 1·54 |
| **3f** | 1·69 | 1·14 | −1·10 | 1·77 | 8·26 |

Table 4. Stabilization energies (kcal mol) of **3b-f** relative to **3a** in a chromophores without helix' arrangement[a], estimates as the difference in heats of formation

| Conformer | AM1 | PM3 | MNDO | MINDO-3 |
|---|---|---|---|---|
| **3a** | 0 | 0 | 0 | 0 |
| **3b** | −0·10 | 0·11 | 0·25 | 0·79 |
| **3c** | 0·28 | −0·31 | 0·38 | 0·03 |
| **3d** | −0·06 | 0·15 | 0·19 | 1·01 |
| **3e** | 4·12 | 2·77 | 12·03 | 19·02 |
| **3f** | 0·26 | 0·12 | 1·20 | 1·12 |

[a] Obtained by removing the helix from the geometrically MM2-optimized conformers (Figures 7–12) while keeping the appended donor and acceptor at fixed positions.

Table 5 Stabilization energies (kcal/mol$^{-1}$) of **3b-f** relative to **3a** in a 'helix without chromophores' arrangement[a], estimated as the difference in heats of formation

| Conformer | AM1 | PM3 | MNDO | MINDO-3 |
|---|---|---|---|---|
| **3a** | 0 | 0 | 0 | 0 |
| **3b** | −4·68 | 0·38 | 4·25 | 3·91 |
| **3c** | −1·74 | 0·63 | 2·79 | 3·76 |
| **3d** | −0·21 | 0·32 | 3·14 | 5·25 |
| **3e** | 1·4 | 0·53 | −3·27 | −2·70 |
| **3f** | −6·00 | −3·00 | −5·60 | −4·17 |

[a] Obtained by removing the appended donor and acceptor from the geometrically optimized conformers (Figures 7–12) while keeping the helix at a fixed position.

Table 6 Stabilization energies (kcal/mol$^{-1}$) of **3b-f** relative to **3a** estimated as the 'addition of helix without chromophores' (Table 5) and the 'chromophores without helix' (Table 4)

| Conformer | AM1 | PM3 | MNDO | MINDO-3 |
|---|---|---|---|---|
| **3a** | 0 | 0 | 0 | 0 |
| **3b** | −4·78 | 0·48 | 4·50 | 4·70 |
| **3c** | −1·46 | 0·32 | 3·17 | 3·79 |
| **3d** | −0·27 | 0·47 | 3·33 | 6·26 |
| **3e** | −1·88 | −0·23 | 6·43 | 14·85 |
| **3f** | 1·66 | 0·65 | −2·07 | −1·58 |

slow and low-yield reaction. For these reasons, we selected a backbone made of alternating L-alanine and $\alpha$-methylalanine amino acid residues. The Aib residue is helix-inducing,[10] and $(Ala–Aib)_n$ peptides are soluble in organic solvents and tend to form $\alpha$-helices when $\mathbf{n}<4$ and the Aib content is <35% (**1** and **2** have a 28% Aib content).[11] The donor and acceptor chromophores were affixed at a position three residues from the helix end to fix their orientation, as the helix ends can sometimes uncoil. An $\alpha$-helix contains 3·7 residues per turn with a unit translational distance of about 5·4 Å.[8] Therefore, in **1** and **2** the two chromophores should be about 10 Å apart if held rigidly and the dihedral angle between groups is held constant.

The right-handled helical conformation of the backbones of **1** and **2** was confirmed by the presence in the CD spectra in acetonitrile of a strong positive band at 190 nm and two negative bands near 210 and 220 nm.[1] Although the pattern and the bands observed in the CD spectra are typical of an $\alpha$-helix,[8] 2D $^1$H NMR techniques are necessary to distinguish between $\alpha$ and $3_{10}$ helical conformations and to estimate better the percentage of helicity in oligopeptides[12] (2D $^1$H NMR spectra were recorded in $CDCl_3$ using a General Electric GN-500 500 MHz spectrometer). 2D $^1$H NMR spectra of **1** and **2** [correlated spectroscopy (COSY) and two-dimensional nuclear Overhauser enhancement spectroscopy (NOESY)[1,13] in $CDCl_3$ showed that both peptides adopt an average $\alpha$-helical conformation on the NMR time-scale. The $\beta$CH($i$)–$\alpha$CH($i+3$) and NH($i$)–NH($i+3$) NOE interactions in both peptides **1** and **2**, shown in the correlation table in Figure 5, are typical of an $\alpha$-helix and are not found in $3_{10}$ helices.

Table 7 Calculated charge-transfer transition energies (eV) in **3a–f**[a]

| Conformer | Transition (eV) | Transition (nm) |
|---|---|---|
| **3a** | 5·029 | 246 |
| **3b** | 5·069 | 245 |
| **3c** | 5·071 | 245 |
| **3d** | 5·168 | 240 |
| **3e** | 4·512 | 275 |
| **3f** | 4·843 | 256 |

[a] The calculated oscillator strength for all charge-transfer transitions is almost zero. Therefore, none of these transitions should be detected in the experimental UV.

Interpretation of NMR spectra in the fast exchange region is limited by the fact that the resonances represent an average of all conformations.[13] By lowering the temperature, it is sometimes possible to slow the exchange sufficiently to see separate resonances for each conformation.[13] $^1$H NMR spectra of **2** in THF at 27, 0, −20, −40, −60 and −80°C are shown in Figure 6. The spectra showed a marked temperature dependence, as all resonances broadened markedly at lower temperatures, in some cases becoming unobservable.

The chemical shift of resonances due to the amide NH groups involved in hydrogen bonding changed dramatically. At lower temperatures the amide peaks resonances, which were not visible or were hidden in the aromatic region, appeared in the region 8·5–9·6 ppm. This may be explained in terms of stronger H-bonding at lower temperature. The chemical shift of the pyrene resonances also changed, and the doublet of the aromatic ring of the dimethylanilino group at 7·25 ppm shifted downfield by 0·20 ppm, whereas the doublet at 6·60 ppm was unchanged. The changes in the NMR spectrum with decreasing temperature, especially the shifts of the aromatic protons of pyrene and aniline, may suggest a conformational change. However, the broadening of the spectrum may also be caused by a slow rate of rotation about the long axis (about 20 Å) of the peptide. (The change in chemical shift, and also the broadening of the spectrum, could also be caused by aggregation of the oligopeptides. However, at −80°C in THF no visible precipitate was observed in the NMR tube.) All spectra collected at even the lowest temperature possible (because of solvent constraints) seem to belong to the intermediate exchange region and separate resonances assignable to each conformation could not be observed under these experimental conditions. For these reasons, the low-temperature NMR experiment is not conclusive in addressing the presence of a variety of conformations.

## CALCULATIONS

To improve our understanding of the conformational distribution in **1** and **2** and the importance of possible through-space interaction between the donor and acceptor groups, force-field and semiempirical calculations were performed on peptide **3**, which incorporates the same appended groups and peptidic backbone as **1**, but without the C- and N-capping groups. This modification was necessary in order to make single-point semiempirical calculations possible by reducing the number of atoms.

### Computational procedure

MM2 force-field calculations were performed in the CAChe system[14] using a Macintosh PowerPC 8100/80. Semiempirical calculations were performed on a Silicon Graphics Indigo2 workstation using the semiempirical program packages AMPAC 2.1[15] and VAMP 4.5.[16] Semiempirical calculations were carried out by using all

available methods: MINDO-3,[17] MNDO,[18] AMI[19] and PM3.[20]

*Force-field calculations*

The dihedral angles A and B (in **3**) were varied from 0 to 360° in 2° steps and each geometry was fully optimized with respect to the two fixed dihedral angles to define possible stable conformers. The six most stable conformations of this grid search were chosen for further optimization, reducing the gradient norm to a reasonably low value (normally 0·0001). Furthermore, the selected six conformations are representative for reasonable orientations of the acceptor and the donor towards each other. In order to obtain information about the possible rotational thresholds, each of these dihedral angles were changed in 1° steps for conformations **3a–f**, in both possible directions, with complete optimization of the remaining degrees of freedom. The energy difference for the starting conformation **3a–f** obtained at a given dihedral angle (at the point before the energy of the system starts to drop, indicating that a possible transition state was passed) was taken as an estimate for a rotational barrier of the chosen bond towards that rotational direction.

The geometries of the conformations **3a–f** are presented as line drawings viewed down and along the helix and as space filling models in Figures 7–12. The calculated heats of formation and estimates for the rotational thresholds thus obtained are given in Table 1.

MM2 force-field calculations predict that the conformation **3a** with the least repulsive steric interaction between the appended groups is preferred (Table 1). Furthermore, structures with an obviously higher strain energy are significantly destabilized (**3b, 3d and 3e**). The energy differences between these conformers, however, are within experimental error, suggesting that in reality these several different conformers probably coexist. Furthermore, the calculated threshold for the rotational barrier suggests a system which is, at least at lower temperature, mainly fixed. Therefore, it is likely that **3** exists as a distribution of different stable ground conformers, without much possiblity for conformational interconversion.

## Semiemprical single-point calculations

Force-field calculations do not yield dipole moments, or even partial changes, because of the classical approach undertaken in this method. *Ab initio* and/or semiempirical quantum mechanical calculations would produce these data, but *ab initio* calculations are not practical for **3** because of the large nubmer of atoms. This is a less significant problem for semiemprical calculations, but even at that level only single-point calculations can be performed. First, semiempirical geometry optimizations are often incapable of reproducing dihedral angles within helical peptides in a satisfactory way,[21] and second, the large number of atoms in **3** makes geometry optimization with conventional workstations impossible. Accordingly, the dipole moments calculated in this way (Table 2), are found not to be dependent either on the conformation or the semiempirical method. We conclude that the weighted conformations of **3** have a net dipole moment greater than 40 D.

Table 3 shows the calculated conformational destabilization of **3b–f** relative to the most stable conformer **3a**. In contrast to the force-field calculations, the semiempirical calculated energies show the sterically more hindered structures to be preferred. This could be the result of a stabilizing through-space and/or through-bond coulostatic interaction between the acceptor and the donor. To obtain more evidence for this conclusion, three calculational procedures were employed:

1. For each conformer the complete helix was removed, while the isolated donor and acceptor are maintained in a fixed geometric relationship (Table 4, chromophore without helix), identical with the energy minima for that conformer. The magnitude of electrostatic through-space interactions could then be calculated for each distance and orientation.
2. The donor and acceptor were removed from each conformer to determine whether distortion of the helix by the appended group can account for the given effect (Table 5, 'helix without chromophores').
3. The sum of the readdition of these two energies was compared with the calculated energy for each conformer to see whether the net energy difference for each conformer **3b–f** could, in addition, provide evidence for a through-bond interaction between donor and acceptor within each conformer.

Examination of the energies thus obtained (Tables 4–6) leads to the following conclusions:

1. The spatial orientation of the 'chromophores without helix' indicates insufficient through-space stabilization in **3b** and **3e** to account for the calculated stabilization. Moreover, **3e** is destabilized by steric hindrance (overlap of van der Waals radii). Hence, through-space interactions alone cannot be responsible for the stabilization of **3e**.
2. Instead, slight modifications in the electronic interactions induced by distortion of the helix exert a remarkable effect on the semiempirical heats of formation.
3. The effect on helix stability is insufficient, however, to account fully for stabilization in **3b–f**. Therefore, the enhanced through-bond interaction that stabilizes the helix must result in enhanced donor–acceptor interactions.

## Calculated charge-transfer transitions

One further important question arises in **3**: is there a low-energy charge-transfer transition between the oriented donor–acceptor pair with a non-zero oscillator strength? To examine this question, limited configuration interaction

 

calculations using AM1 with six virtual and six occupied orbitals were performed (only single and double excited configurations were taken into account). These calculations yield full absorption spectra of **3a**–**f**, but only the HOMO-donor to LUMO-acceptor transitions are shown in Table 7.

These calculations show that conformation exerts a remarkable influence on the transition energy, but that the calculated oscillator strength of these transitions is very weak for **3a**–**f**. According to these calculations, no ground-state charge-transfer absorption should be detectable in any kind of absorption spectra, and indeed none is observed.

## CONCLUSIONS

Different rates of photoinduced electron transfer are observed upon laser flash excitation of peptides **1** and **2**, producing a charge-separated ion pair. This observation provides strong evidence for the influence of the macroscopic electric dipole of the helix on electronic coupling between the appended donor and acceptor. Force-field calculations, NMR experiments and time-resolved single-photon counting experiments offer evidence for the presence of different side-chain confomers in **1** and **2**, which complicate the interpretation of observed optical and lifetime data. Furthermore, semiempirical single-point calculations demonstrate the possibility that through-bond, rather than through-space, interactions constitute a principal electronic interaction between the appended chromophores. Even though the model peptide **3** has only a small number of degrees of freedom, the side-chain conformational flexibility of the appended groups causes significant complexity in the interpretation of the experimental observations. Further experiments to synthesize a completely rigid $\alpha$-helical peptide are in progress.

### ACKNOWLEDGMENTS

This work was supported by the US Department of Energy, Office of Basic Energy Science. A. K. thanks the DFG (Deutsche Forschungsgemeinshaft) for a research stipend.

## REFERENCES

1. E. Galoppini and M. A. Fox, *J. Am. Chem. Soc*. **118**, 2299 (1996).
2. (a) W. G. J. Hol, *Prog. Biophys. Mol. Biol*. **45**, 149 (1985); (b) W. G. J. Hol, P. T. van Duijnen and H. J. C. Berendsen, *Nature* (London) **273**, 443 (1978); (c) A. Wada, *Adv. Biophys.* **9**, 1 (1976); (d) R. J. Abraham, B. D. Hudson, W. A. Thomas and A. Krohn, *J. Mol. Graphics* **4**, 28 (1986).
3. (a) H. M. Brothers, III, J. S. Zhou and N. M. Kostic, *J. Inorg. Organomet. Polym.* **3**, 59 (1993); (b) D. J. Lockhart and P. S. Kim, *Science* **257**, 947 (1992); (c) G. Alegria and P. L. Dutton, *Biochim. Biophys. Acta.* **234**, 1057, 258 (1991).
4. (a) D. Gosztola, H. Yamada and M. R. Wasielewski, *J. Am. Chem. Soc.*, **117**, 2041 (1995); (b) S. Franzen, K. Lao and S. G. Boxer, *Chem. Phys. Lett.* **197**, 380 (1992); (c) S. G. Boxer, D. J. Lockhart and S. Franzen, in *Photochemical Energy Conversion*, edited by J. R. Norris and D. Meisel, Chap. 2.4. Elsevier, Amsterdam (1989); (d) S. G. Boxer, R. A. Goldstein and S. Franzen, in *Photoinduced Electron Transfer Part B. Experimental Techniques and Medium Effect*, edited by M. A. Fox and M. Channon, p. 163. Elsevier, Amsterdam (1988); (e) A. Warshel and J. Åqvist, *Annu. Rev. Biophys. Chem.* **20**, 267 (1991).
5. (a) H. Schomburg, H. Staerk and A. Weller, *Chem. Phys. Lett.* **22**, 1 (1973); (b) **22**, 433 (1973).
6. *Handbook of Photochemistry*, p. 123. Marcel Dekker, New York (1993).
7. (a) B. Pispisa, M. Venanzi, A. Palleschi and G. Zanotti, *Macromolecules* **27**, 7800 (1994); (b) Y. Inai, M. Sisido and Y. Imanishi, *J. Phys. Chem.* **95**, 3847 (1991); (c) Y. Inai, M. Sisido and Y. Imanishi, *J. Phys. Chem.* **94**, 6237 (1990); (d) G. Basu, M. Kubasik, D. Anglos, B. Secor and A. Kuki, *J. Am. Chem. Soc.* **112**, 9410 (1990); (e) M. Sisido, R. Tanaka, Y. Inai and Y. Imanishi, *J. Am. Chem. Soc.* **111**, 6790 (1989); (f) A. Vassilian, J. F. Wishart, B. van Hemelryck, H. Schwarz and S. S. Isied, *J. Am. Chem. Soc.* **112**, 7278 (1990).
8. M. Goodman, A. Verdini, N. Choi and S. Masuda, *Top. Stereochem.* **5**, 69 (1970).
9. M. S. Meier, M. A. Fox and J. R. Miller, *J. Org. Chem.* **56**, 5380 (1991).
10. G. R. Marshall, E. E. Hodgkin, D. A. Langs, G. D. Smith, J. Zabrocky and M. T. Leplawy, *Proc. Natl. Acad. Sci. USA* **87**, 487 (1990).
11. (a) K. Oyoda, Y. Kitakawa, S. Kimura and Y. Imanishi, *Biopolymers* **33**, 1337 (1993); (b) I. L. Karle, M. Sukuman and P. Balaram, *Proc. Natl. Acad. Sci. USA* **83**, 9284 (1986).
12. (a) K. Wütrich, *NMR of Proteins and Nucleic Acids*, Chap. 7. Wiley, New York (1986); (b) W. R. Croasman and R. M. K. Carlson, *2-D NMR Spectroscopy.* VCH, Weinheim (1994).
13. L.-Y. Lian and G. C. K. Roberts, in *NMR of Macromolecules: a Practical Approach*, edited by G. C. K. Roberts, Chap. 6, Oxford University Press, Oxford (1993).
14. *CACHE Scientific, Version 3.7*. CAChe Scientific (1994).
15. D. A. Liotard, E. F. Healy, J. M. Ruiz and M. J. S. Dewar, *AMPAC*. University of Texas at Austin, Austin, TX (1989).
16. G. Rauhut, A. Alex, J. Chandrasekhar and T. Clark. *VAMP4.5*. Oxford Molecular, Oxford (1993).
17. (a) R. C. Bingham, M. J. S. Dewar and D. H. Lo, *J. Am. Chem. Soc*. **97**, 1285, 1294, 1302, 1307 (1975); (b) M. J. S. Dewar, D. H. Lo and C. A. Ramsden, *J. Am. Chem. Soc*. **97**, 1311 (1975).
18. M. J. S. Dewar and W. J. Thiel, *J. Am. Chem. Soc.* **99**, 4899 (1977).
19. M. J. S. Dewar, E. G. Zoebisch, E. F. Healy and J. J. P. Stewart, *J. Am. Chem. Soc.* **107**, 3902 (1985).
20. J. J. P. Stewart, *J. Comput. Chem.* **10**, 209 (1989).
21. (a) T. Clark, *A Handbook of Computational Chemistry.* Wiley, New York (1985); (b) J. J. P. Stewart, *The MOPAC Manual*, QCPE 455. Department of Chemistry, Indiana University, Bloomington, IN.

 